5-2009

Clinical Field-strength MRI of Amyloid Plaques Induced by Low-level Cholesterol Feeding in Rabbits

John A. Ronald
Robarts Research Institute, jronald@imaging.robarts.ca

Yuanxin Chen
Robarts Research Institute, ychen@imaging.robarts.ca

Lisa Bernas
Robarts Research Institute

Hagen H. Kitzler
Robarts Research Institute, hkitzler@imaging.robarts.ca

Kem A. Rogers
University of Western Ontario, kem.rogers@schulich.uwo.ca

See next page for additional authors

Authors

John A. Ronald, Yuanxin Chen, Lisa Bernas, Hagen H. Kitzler, Kem A. Rogers, Robert A. Hegele, and Brian K. Rutt

BRAIN

Clinical field-strength MRI of amyloid plaques induced by low-level cholesterol feeding in rabbits

John A. Ronald,[1,2] Yuanxin Chen,[1] Lisa Bernas,[1,2] Hagen H. Kitzler,[1,3] Kem A. Rogers,[4] Robert A. Hegele[1] and Brian K. Rutt[1,2,3,5]

1 Robarts Research Institute, University of Western Ontario, London, ON, Canada
2 Department of Medical Biophysics, University of Western Ontario, London, ON, Canada
3 Department of Diagnostic Radiology and Nuclear Medicine, University of Western Ontario, London, ON, Canada
4 Department of Anatomy and Cell Biology, University of Western Ontario, London, ON, Canada
5 Department of Radiology, Stanford University, Palo Alto, California, USA

Correspondence to: John A. Ronald,
Robarts Research Institute,
University of Western Ontario,
100 Perth Drive, 1st Floor,
London, ON, Canada N6A 5K8
E-mail: jronald@imaging.robarts.ca

Two significant barriers have limited the development of effective treatment of Alzheimer's disease. First, for many cases the aetiology is unknown and likely multi-factorial. Among these factors, hypercholesterolemia is a known risk predictor and has been linked to the formation of β-amyloid plaques, a pathological hallmark this disease. Second, standardized diagnostic tools are unable to definitively diagnose this disease prior to death; hence new diagnostic tools are urgently needed. Magnetic resonance imaging (MRI) using high field-strength scanners has shown promise for direct visualization of β-amyloid plaques, allowing *in vivo* longitudinal tracking of disease progression in mouse models. Here, we present a new rabbit model for studying the relationship between cholesterol and Alzheimer's disease development and new tools for direct visualization of β-amyloid plaques using clinical field-strength MRI. New Zealand white rabbits were fed either a low-level (0.125–0.25% w/w) cholesterol diet ($n = 5$) or normal chow ($n = 4$) for 27 months. High-resolution ($66 \times 66 \times 100\,\mu m^3$; scan time $= 96$ min) *ex vivo* MRI of brains was performed using a 3-Tesla (T) MR scanner interfaced with customized gradient and radiofrequency coils. β-Amyloid-42 immunostaining and Prussian blue iron staining were performed on brain sections and MR and histological images were manually registered. MRI revealed distinct signal voids throughout the brains of cholesterol-fed rabbits, whereas minimal voids were seen in control rabbit brains. These voids corresponded directly to small clusters of extracellular β-amyloid-positive plaques, which were consistently identified as iron-loaded (the presumed source of MR contrast). Plaques were typically located in the hippocampus, parahippocampal gyrus, striatum, hypothalamus and thalamus. Quantitative analysis of the number of histologically positive β-amyloid plaques ($P < 0.0001$) and MR-positive signal voids ($P < 0.05$) found in cholesterol-fed and control rabbit brains corroborated our qualitative observations. In conclusion, long-term, low-level cholesterol feeding was sufficient to promote the formation of extracellular β-amyloid plaque formation in rabbits, supporting the integral role of cholesterol in the aetiology of Alzheimer's disease. We also present the first evidence that MRI is capable of detecting iron-associated β-amyloid plaques in a rabbit model of Alzheimer's disease and have advanced the sensitivity of MRI for plaque detection to a new level, allowing clinical field-strength scanners to be employed. We believe extension of these technologies to an *in vivo* setting in rabbits is feasible and that our results support future work exploring the role of MRI as a leading imaging tool for this debilitating and life-threatening disease.

Introduction

Alzheimer's disease is a progressive neurodegenerative disorder that is the dominant cause of dementia in the elderly. It is characterized by the accumulation of extracellular β-amyloid rich plaques and intraneuronal neurofibrillary tangles, neuronal dysfunction and death, and a gradual deterioration in cognition, function and behaviour (Khachaturian, 1985). In developed countries, the prevalence of Alzheimer's disease doubles with each passing decade of life such that ~5–8% of 65 year olds have this disease, whereas 30% of 85 year olds are affected (Petrella et al., 2003; Villemagne et al., 2005). As individuals are now more likely to live to and beyond the age of Alzheimer's disease onset, its incidence is expected to triple over the next 50 years (Carr et al., 1997).

Two main challenges exist in the effective treatment of Alzheimer's disease. First, the aetiology of the disease remains elusive. While genetic abnormalities appear to be responsible for a small number of familial early-onset cases, the cause of the vast number of sporadic late-onset cases is unknown (Canevari and Clark, 2007). Sporadic Alzheimer's disease is thought to have multiple causes, however, numerous lines of evidence point to a leading role of cholesterol metabolism. The $\varepsilon 4^+/\varepsilon 4^+$ genotype for apolipoprotein E, the major cholesterol carrier in the central nervous system, is the strongest independent risk factor for late-onset Alzheimer's disease (Corder et al., 1993). Hypercholesterolemia increases the risk of Alzheimer's disease in later life (Kivipelto et al., 2001a, b; Pappolla et al., 2003; Whitmer et al., 2005). Cholesterol regulates the production of Aβ and influences Aβ toxicity to neurons (Simons et al., 1998; Yip et al., 2001; Curtain et al., 2003; Ehehalt et al., 2003). Statins (cholesterol-lowering drugs) may decrease the risk of developing Alzheimer's disease (Wolozin et al., 2000; Li et al., 2007) and improve cognition and behaviour in mild Alzheimer's disease patients (Sparks et al., 2005). Finally, there is an association between atherosclerosis, for which cholesterol is a key risk factor, and late-life dementia (Sparks et al., 1990; Hofman et al., 1997).

The second challenge is that standardized ante-mortem assessment of the cognitive status of individuals does not always match the pathological findings at autopsy (Hulette et al., 1998; Morris and Price, 2001; Knopman et al., 2003; Jicha et al., 2006). For this reason, definitive diagnosis of Alzheimer's disease has traditionally required post-mortem pathological assessment of brain tissue, emphasizing the need for new methods of identifying this disease prior to death. Of particular, interest is the development of neuroimaging techniques that can directly visualize β-amyloid plaques since these plaques are formed long (potentially decades) before the clinical manifestation of the disease. This would allow earlier, definitive diagnosis to be possible and direct the use of appropriate, effective treatments at the earliest disease stages. Magnetic resonance imaging (MRI) has shown significant progress towards reaching this goal. Direct MR visualization of β-amyloid plaques without contrast agents has been accomplished in both ex vivo brain samples from Alzheimer's disease patients (Benveniste et al., 1999) and in vivo in various transgenic mouse models of Alzheimer's disease (Jack et al., 2004, 2005; Vanhoutte et al., 2005; Braakman et al., 2006). This latter development is particularly significant as this can allow the tracking of disease throughout the whole brain in individual animals over time. Importantly, two pre-requisites for successfully visualizing β-amyloid plaques are thought to be the presence of magnetic-susceptibility-perturbing iron within the plaques and the use of high field-strength MR scanners [7 or 9.4 Tesla (T)] capable of generating the high-resolution, high signal-to-noise ratio (SNR) images (micro-MRI) (Jack et al., 2004; Wadghiri et al., 2004; Vanhoutte et al., 2005). While these studies represent major advances for the study of Alzheimer's disease in small animals, to date these technologies have not been applied to larger animal models of this disease, nor has direct β-amyloid plaque visualization been possible using clinical-grade MR scanners, which is an important goal for future clinical translation.

The work presented here is the result of the serendipitous convergence of two previously unrelated lines of research by our group. First, we have been studying rabbits fed a low-level cholesterol diet for extended periods of time as a model of atherosclerosis (Daley et al., 1994a, b; Ronald et al., 2007). Here, we demonstrate that this diet also promotes the deposition of iron-rich β-amyloid plaques in the brains of these animals, providing a unique larger animal model useful for studying the influence of cholesterol on the initiation and progression/regression of Alzheimer's disease. Second, we have recently shown that clinical field-strength MRI can be used to non-invasively visualize iron-loaded cells down to the single cell level in mouse brain (Heyn et al., 2006a). Here we have optimized this technology, allowing direct visualization of the iron-rich β-amyloid plaques formed in our rabbit model. While we do not contend that our MRI methods are immediately translatable to the clinic, we feel that this is a significant technological advancement in the sensitivity of MRI for direct detection of plaques, which points to MRI's potential for aiding in the study, and potentially diagnosis, of this debilitating and life-threatening disease.

Methods

Animal model

Animals were cared for in accordance with guidelines of the Canadian Council on Animal Care. Five New Zealand white rabbits (Charles River Laboratories, Inc. Wilmington, MA) were fed 100 g/day of rabbit chow

supplemented with either 0.125 or 0.25% w/w cholesterol. Four additional age-matched rabbits were fed normal chow and served as controls [normal chow contained <0.001% (w/w) cholesterol]. Three of these control animals were purchased from the breeder at 22 months of age. These rabbits were fed normal rabbit chow by the breeder during the first 22 months and maintained on this diet once purchased. Serum cholesterol levels were determined for each animal. Blood was drawn from the central ear artery following Acepromazine administration (0.10 ml/kg intramuscular) to promote arterial dilation and analgesia. Samples were mixed with ethylene-diamine tetra-acetic acid to a final concentration of 0.15% (w/v) and serum was collected by centrifugation at 5000 r.p.m. for 15 min at 4°C. Total serum cholesterol was measured using a colorimetric enzyme-based kit (Wako Diagnositics, Richmond, VA).

Tissue collection

Animals were sacrificed with an overdose of ketamine (2 ml intravenous bolus) and pressure-perfused via the left ventricle with a minimum of 1.5 l of heparinized (1 U/ml) Hanks' balanced salt solution. Brains were then carefully dissected and cut down the midline. One hemisphere from each rabbit was immersed in 10% formalin for 48 h at 4°C and switched to phosphate buffered saline at 4°C until imaging.

MRI protocol

Half brains were immersed in a proton-free perfluorocarbon liquid (Fluorinert FC-72, 3M, St Paul, MN) and scanned using a 3 T whole-body MR system. In order to collect high-resolution and high signal-to-noise ratio (SNR) images (required to visualize β-amyloid plaques) using a clinical field-strength scanner, we utilized two custom-built pieces of MR hardware. First, high-resolution imaging was achievable by using an insertable gradient coil (inner diameter of 17.5 cm) capable of producing a peak gradient strength (500 mT/m) and peak slew rate (3200 T/m/s) more than a factor of 10 higher than corresponding values for the whole-body gradient coil on the 3 T system (gradient strength and slew rate = 40 mT/m and 150 T/m/s, respectively). Second, to collect high SNR images a solenoidal radiofrequency coil (2 cm inner diameter) that fit closely around each immersed half brain was used. Furthermore, high SNR, in addition to high sensitivity to iron in plaques, was also achieved through use of the three-dimensional fast imaging employing steady state acquisition (3DFIESTA) pulse sequence. This sequence has previously been explored in our laboratory for high-resolution, high-SNR imaging of single iron-loaded cells both *in vitro* and *in vivo* (Foster-Gareau *et al*., 2003; Heyn *et al*., 2005; Heyn *et al*., 2006a). Sagittal MR images of each brain were acquired at a resolution of $66 \times 66 \times 100\,\mu m^3$ using 3DFIESTA (repetition time = 20 ms; echo time = 10 ms; flip angle = 20°; bandwidth = ±18 kHz; phase cycling number/recon = 10/sum-of-squares; scan time = 96 min).

Histology

Following MRI, 40 μm sagittal free-floating sections of each brain were collected. Sections were treated with 10% formic acid (pH 1.6) for 20 min. Immunostaining was performed using a mouse anti-human β-amyloid 1–16 primary antibody (1:150 dilution; stains Alzheimer's senile plaques; Chemicon International, Temecula, CA), a horse anti-mouse biotinylated secondary antibody (1:300 dilution; Vector Laboratories, Burlington, ON), processed using an ABC-HRP complex

solution for 30 min (Vector Laboratories, Burlington, ON), and visualized with 3′-diaminobenzidine (0.5 mg/ml; Sigma-Aldrich Canada, Oakville, ON). Negative control staining (without addition of primary antibody) was performed on adjacent sections. Sections were air dried onto slides and images were taken using a Zeiss Axioplan 2ie microscope (Carl Zeiss Canada, Toronto, ON). Subsequently, Prussian blue iron staining was performed on each β-amyloid-stained section and reimaged to visualize iron accumulation and its association with β-amyloid-positive regions. Slides were further scanned using a Epson Expression 1680 flat-bed scanner (Model G7808; Epson Canada Limited; Toronto, ON) to generate low-magnification images of each brain section. Finally, the position of each β-amyloid- and iron-positive plaque was marked on the scanned image and this map of histologically positive plaques was manually registered to its corresponding sagittal MR slice using anatomical landmarks (see below). Regions of well-defined signal loss (signal voids) within the MR slice were identified and marked with the person blinded to the histology results.

MR and histological image analysis

Manual counting of β-amyloid plaques and signal voids was performed in histological and MR datasets, respectively. For histology, the total number of regions containing iron-loaded, β-amyloid-positive plaques in seven brain sections (spaced 1 mm apart) from each rabbit was determined. A positive region was defined as having one or more plaques spaced closely together (within 100 μm). Corresponding MR slices were selected by matching at least three anatomic landmarks between histological images and MR images. Specifically, we compared the formation and shape of the following central brain structures: the caudate nucleus, the thalamus and the hippocampus. Signal voids were defined as small image objects characterized by a distinct focal MR hypointensity compared with its surrounding tissue area. Extreme caution needed to be applied in order to not mistake intra-parenchymal voids descending from plaques with those caused by near-surface air remnants or paramagnetic remains of blood within vessels (minimized due to perfusion). Therefore, we applied the following rules during quantitation: (i) voids were sharply bounded hypointense objects of round shape; (ii) voids needed to feature an intra-parenchymal localization; and (iii) to avoid partial volume effects, voids needed to exhibit at least a distance of one diameter of their own size from specimen surfaces or ventricles. Two independent raters (JAR, HHK) counted the number of voids in the selected MR images. A conjoint quantification of voids by both raters was also performed. Void location was also recorded as to whether it was clearly present in grey matter or white matter or in parenchymal locations with no clear distinction between grey and white matter (referred to as mixed), like brainstem or basal ganglia.

Statistical analysis

For comparisons of MR and histological data between cholesterol-fed and control groups two-tailed *t*-tests were performed. For comparisons of void locations in cholesterol-fed animal brains, a one-way analysis of variance (ANOVA) followed by a *post hoc* Tukey's multiple comparison test was performed. Both Pearson correlational and Bland-Altman analyses were performed to assess inter-rater variability for void counting. For all tests, the nominal level of significance was $P < 0.05$. GraphPad Prism 4.0a (GraphPad Software Inc., San Diego, CA) was used for statistical analysis.

Results

High-resolution MRI revealed distinct signal voids throughout the brains of rabbits fed a long-term, low-level cholesterol diet

Our cholesterol diet regimen was originally proposed to promote the formation of lipid-rich atherosclerotic aortic plaques in New Zealand white rabbits (Daley *et al.*, 1994a, b; Ronald *et al.*, 2007). This diet starts with feeding rabbits a 0.25% w/w cholesterol-diet for a minimum of 7 months during which time the average serum cholesterol levels rose ~1000 mg/dl above baseline (Table 1). Following this induction period, the cholesterol level is titrated between 0.125% and 0.25% to maintain an average serum cholesterol level above 400 mg/dl whilst preventing liver failure due to excessive cholesterol accumulation and toxicity.

In contrast, serum cholesterol levels in control animals was significantly lower (average control = 31.75 mg/dl versus average cholesterol-fed = 668.11 mg/dl; $P < 0.001$ at 21–27 months).

Before any histological results were attained, high-resolution ($66 \times 66 \times 100 \mu m^3$) *ex vivo* MRI (or micro-MRI) of perfused, fixed half brains from both cholesterol-fed and control rabbits was performed (Fig. 1). Signal voids were apparent in MR images throughout the brains of cholesterol-fed rabbits (Fig. 1A). Importantly, minimal signal voids were seen in images of control rabbit brains (Fig. 1B).

MR signal voids corresponded to iron-loaded, β-amyloid-positive extracellular plaques formed as a result of cholesterol-feeding

β-Amyloid immunostaining revealed the presence of extracellular β-amyloid-rich plaques throughout the brains of cholesterol-fed

Table 1 Total serum cholesterol levels (mg/dl) of cholesterol-fed and control rabbits over time

Diet	Baseline	1–7 months	8–13 months	14–20 months	21–27 months
Cholesterol-fed	64.85 ± 22.33 ($n = 5$)	1061.20 ± 413.98 ($n = 5$)	428.09 ± 247.38 ($n = 5$)	422.20 ± 221.26 ($n = 5$)	668.11 ± 230.12[#] ($n = 5$)
Control	26 ($n = 1^a$)	31 ($n = 1^a$)	18 ($n = 1^a$)	17 ($n = 1^a$)	31.75 ± 12.47 ($n = 4$)

Values represent mean ± SD.
a Three age-matched control animals were acquired from breeder at 22 months old.
[#] $P < 0.001$ when compared with control animal values at 21–27 months.
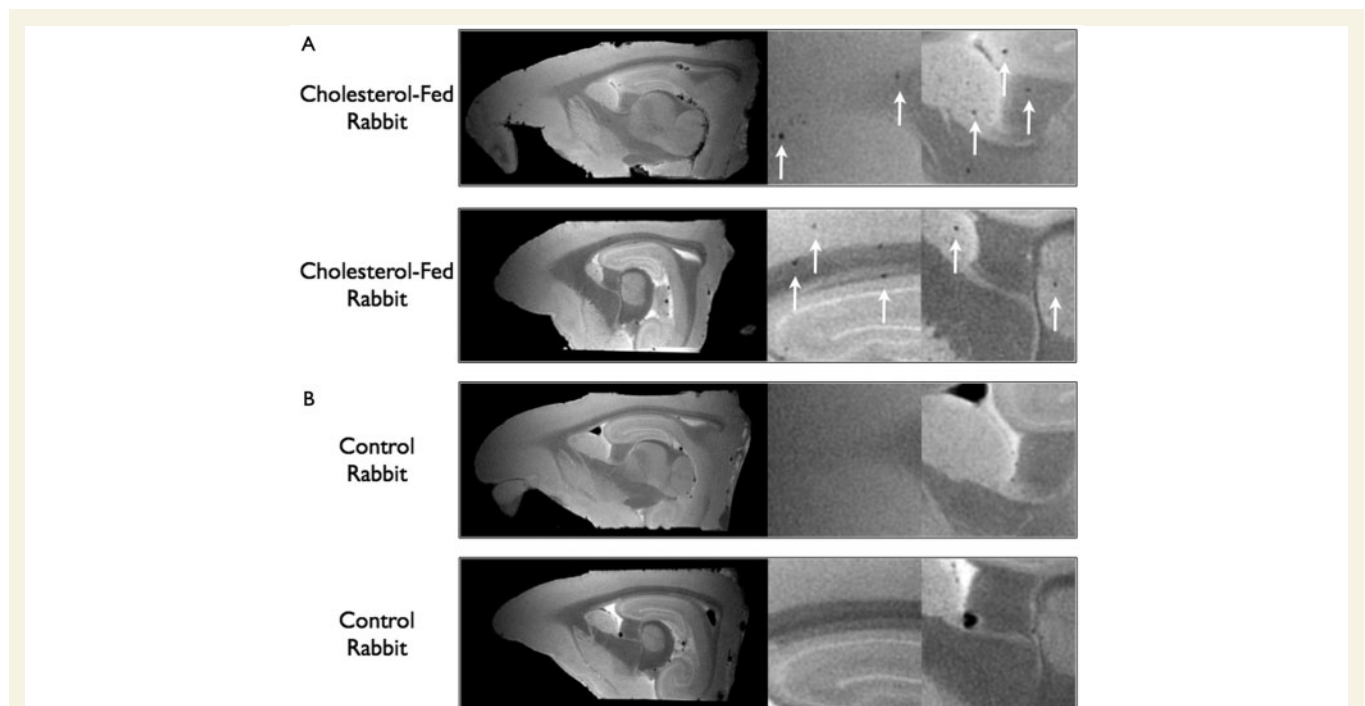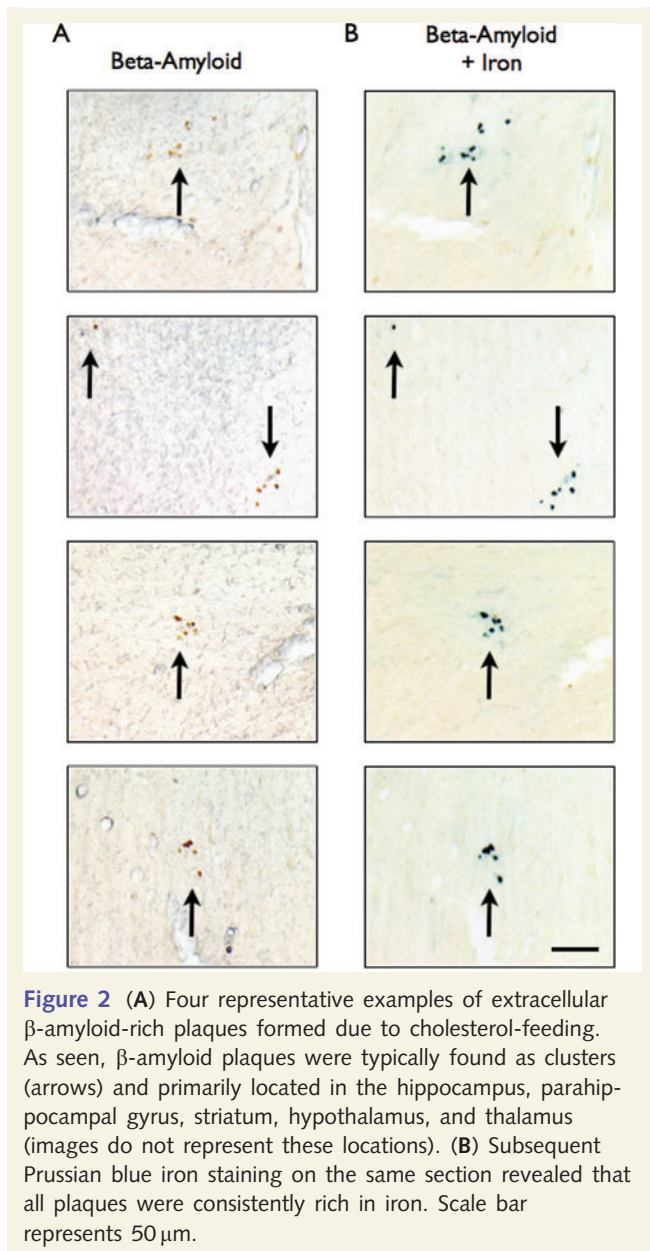

Figure 1 High-resolution ($66 \times 66 \times 100 \mu m^3$) *ex vivo* MR images of cholesterol-fed (**A**) and control (**B**) rabbit brains. Images of two different animals from each rabbit group are shown in (**A**) and (**B**). Each row of images represents an individual animal with a low magnification sagittal image on the left followed by two magnified views on the right to better visualize differences between groups. Distinct signal voids were clearly seen throughout the brains of cholesterol-fed rabbits (**A**). Minimal voids were detectable in the parenchyma of the brains from control rabbits (**B**).

Figure 2 (**A**) Four representative examples of extracellular β-amyloid-rich plaques formed due to cholesterol-feeding. As seen, β-amyloid plaques were typically found as clusters (arrows) and primarily located in the hippocampus, parahippocampal gyrus, striatum, hypothalamus, and thalamus (images do not represent these locations). (**B**) Subsequent Prussian blue iron staining on the same section revealed that all plaques were consistently rich in iron. Scale bar represents 50 μm.

plaques confirmed by histology corresponded to the signal voids identified by MRI (Fig. 4), and therefore we conclude that these plaques cause the MR-visible signal voids. As shown in a representative comparison in Fig. 4, many of the plaque clusters (white numbers) were readily visualized in the corresponding MR image as distinct signal voids. Of note, several histologically detected plaques (red numbers) were not seen as a void in the corresponding MR image, however, we found that these plaques were typically much smaller and singular in nature compared to MR-visible plaques.

Quantitation of the histological and MR datasets corroborated our qualitative observations. Significantly more plaque-positive regions were detected in the histological sections of brains from rabbits fed the cholesterol-supplemented diet than normal chow (Fig. 4A; $P < 0.0001$). Because signal loss in MRI can be caused by other non-plaque effects (e.g. incomplete perfusion leaving blood products or air) some ambiguity can arise when manually counting signal voids. Therefore, two independent raters counted voids within the same selected set of MR slices. Both raters independently counted significantly more signal voids in brains from cholesterol-fed animals than control animals (data not shown). However, a significantly positive weak correlation was found ($R^2 = 0.3561$; $P < 0.0001$) between the two raters and Bland-Altman analysis revealed that there was a slight bias between the raters for the number of voids counted in slices with many voids (Supplementary Fig. S1). Due to this, a consensus void count was performed. This revealed that significantly more signal voids were identified in MR images of brains from cholesterol-fed rabbits than control rabbits (Fig. 4B; $P = 0.0143$). Finally, no preferential location for the MR signal voids within brains from cholesterol-fed animals was found (Fig. 4C).

Discussion

This study reveals that feeding New Zealand white rabbits a low-level cholesterol diet for extended periods of time is sufficient to promote the formation of extracellular β-amyloid plaques resembling those found in Alzheimer's disease patients. As plasma cholesterol has repeatedly been shown to be a risk factor of Alzheimer's disease for at least 20 years (Sparks *et al.*, 1990; Corder *et al.*, 1993; Hofman *et al.*, 1997; Simons *et al.*, 1998; Wolozin *et al.*, 2000; Kivipelto *et al.*, 2001a, b; Yip *et al.*, 2001; Curtain *et al.*, 2003; Ehehalt *et al.*, 2003; Pappolla *et al.*, 2003; Sparks *et al.*, 2005; Whitmer *et al.*, 2005; Li *et al.*, 2007), we are convinced that future study of this model will lead to consolidation and further understanding of the relationship between cholesterol and β-amyloid plaque deposition. Along with this exciting discovery, we have found that these plaques are consistently loaded with iron. As a result of this, many of these plaques can be directly visualized as signal voids in MR images. While the concept of visualizing iron-loaded β-amyloid plaques using MRI has previously been demonstrated in transgenic mouse models (Jack *et al.*, 2004, 2005; Vanhoutte *et al.*, 2005; Braakman *et al.*, 2006), we believe our work represents the first successful attempt at visualizing plaques in a larger and non-transgenic, spontaneous Alzheimer's disease animal model. Of importance is that while our imaging was performed on
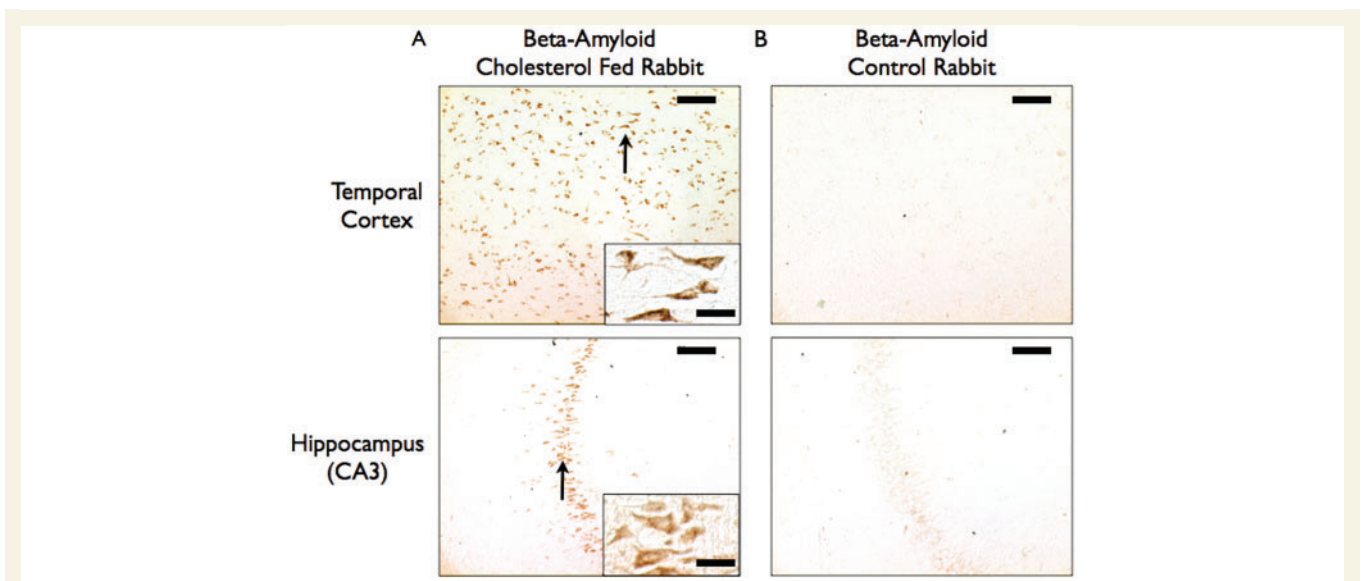
rabbits (Fig. 2A). Small β-amyloid-positive plaques (~10 μm in diameter) were typically found in clusters within various regions of the brain including the hippocampus, parahippocampal gyrus, striatum, hypothalamus and thalamus. No positive staining was found in negative control stained sections (not shown). Important for MR detectability, subsequent Prussian blue staining for iron showed that all plaques found were also rich in iron (Fig. 2B). Similar to previous findings seen with high-level (2%), short-term (10 weeks) cholesterol diets (Sparks *et al.*, 1994), the low-level (0.125–0.25%), long-term (28 months) cholesterol regimen used here also promoted intraneuronal β-amyloid accumulation in various regions of the brain including the temporal and frontal cortices, caudate putamen, striatum and hippocampus. Representative examples of hippocampal and temporal cortex positive staining are shown in Fig. 3.

Registration between histological images of brain sections and MR images of half brains showed that iron-loaded, β-amyloid-positive

Fig. 3 Increased intraneuronal β-amyloid accumulation was detected in the brains of cholesterol-fed rabbits (**A**), but not in control rabbits (**B**). Top and bottom images represent positive intracellular staining found in the temporal cortex and CA3 region of the hippocampus, respectively. Insets in (**A**) are higher magnification of regions indicated by arrows. Scale bars in low- and high-magnification images represent 100 and 20 μm, respectively.
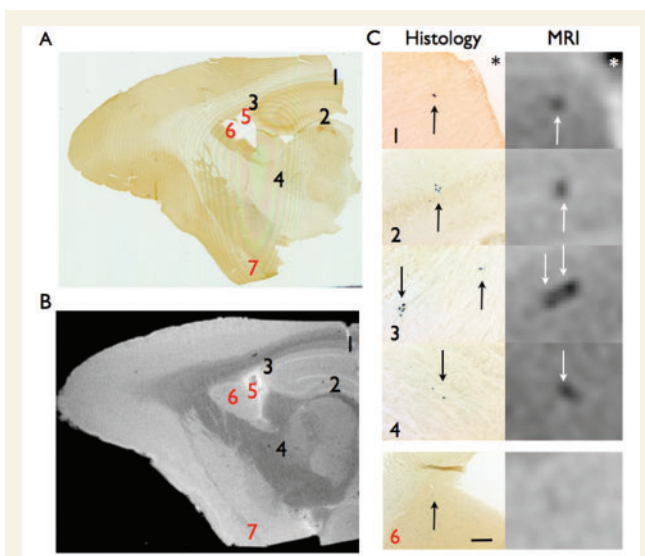

Figure 4 (**A**) Histological brain section stained for both β-amyloid and iron from a 29-month–old rabbit fed cholesterol-diet for 27 months. The locations of seven iron-loaded, β-amyloid-rich plaque clusters are indicated. (**B**) Corresponding MR image with the identified locations of the histologically confirmed plaques superimposed. Four of the seven plaque clusters were visualized as signal voids in the MR image (black numbers). The other three plaques (red numbers) were not seen as voids in the MR image. (**C**) Higher magnification of both the histology and MRI revealed that visible plaques were typically large, singular plaques (location 1) or clusters of small plaques (locations 2–4), whereas voids not seen in MRI were singular and notably smaller (location 6). Asterisks in 1 indicate areas outside of brain. Scale bar represents 50 μm.

ex vivo specimens, we are confident that *in vivo* non-invasive imaging of plaques is feasible in the future since the scan time used here (96 min) is well within the anaesthesia limits of this animal model (~4 h). Finally, an important feature of this work has been the use of a clinical-field strength (3 T) scanner, representing a significant advancement in the sensitivity of MRI for the direct detection of β-amyloid plaques. This lends further support to the role of MRI as a leading modality in the study and diagnosis of Alzheimer's disease.

While we found that cholesterol feeding promoted β-amyloid plaque deposition, it should be noted that this concept is not entirely novel. Sparks *et al*. (1994) were the first to show that feeding rabbits a high-cholesterol (2% w/w) diet promoted the deposition of β-amyloid in rabbits. As highlighted by Sparks and Schreurs (2003), this is considered a highly valuable Alzheimer's disease model since it displays many of the pathological brain changes seen in Alzheimer's disease patients. This includes evidence of intraneuronal (Sparks *et al*., 1994) and extracellular β-amyloid immunoreactivity (Sparks *et al*., 1994; Sparks and Schreurs, 2003); microgliosis and apoptosis (Streit and Sparks, 1997); and deficiency in the ability to learn a difficult task (Sparks and Schreurs, 2003). Despite the advantages of the cholesterol-fed rabbit model, two significant drawbacks of the high-level cholesterol diets used in the past are noteworthy. First, the majority of β-amyloid deposition found in the original Sparks study (Sparks *et al*., 1994) was intraneuronal with only one rabbit showing signs of extracellular β-amyloid deposition, the pathognomonic hallmark of Alzheimer's disease. Second, high-level cholesterol feeding can only be maintained for short periods of time. After ~8 weeks on a 2% cholesterol diet, rabbits often succumb to liver and renal failure (Sparks *et al*., 1994). It has been shown that cholesterol feeding and supplementation of drinking water
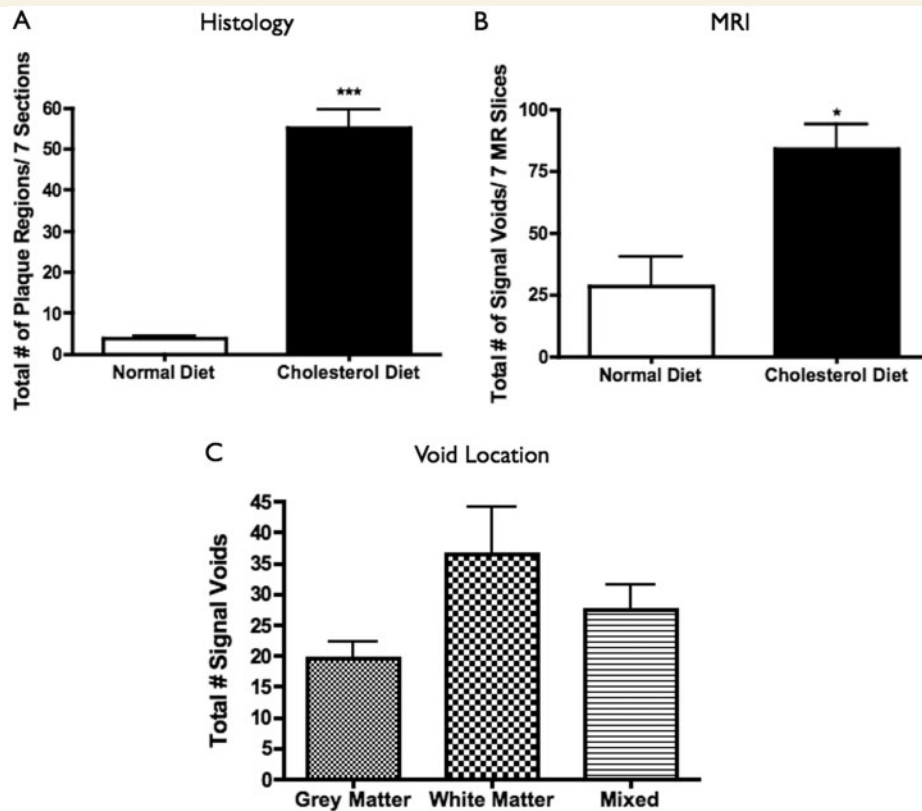
Figure 5 (**A**) Histological analysis of β-amyloid plaque burden revealed that significantly more plaques were seen in cholesterol-fed than control rabbit brain sections (***$P < 0.0001$). (**B**) Similarly, consensus MR void analysis confirmed significantly more voids in rabbits fed cholesterol-enriched diets compared with controls (*$P < 0.05$). (**C**) No differences in void location (grey matter, white matter or mixed—regions with no clear distinction between grey matter and white matter) were seen in MR images from brains of cholesterol-fed rabbits.

with copper can improve extracellular β-amyloid deposition (Sparks and Schreurs, 2003), however, this does not lower animal mortality rates. Our diet regimen addresses both drawbacks since all animals fed the low-level (0.125–0.25%) cholesterol diet developed extracellular β-amyloid plaques, and the more gradual titration of serum cholesterol levels over time prevented premature death of the animals. This survivable cholesterol-fed rabbit model should allow the testing of treatment efficacy after having established a known β-amyloid plaque burden, and also may more closely reflect the natural history of Alzheimer's disease in humans since plaque development occurs over years, even decades.

Currently, ante-mortem Alzheimer's disease diagnosis is largely based on clinical examination, performance on standardized cognitive tests, and the use of structural neuroimaging. MRI is useful for detecting late-stage brain atrophy due to neuronal loss and can also report on neurofibrillary tangle burden during the progression of Alzheimer's disease (Jack *et al.*, 1992; Gosche *et al.*, 2002; Jack *et al.*, 2002; Schott *et al.*, 2005; Vemuri *et al.*, 2008). Unfortunately, clinical MRI measures do not correlate well with β-amyloid plaque burden (Josephs *et al.*, 2008) and a non-invasive technique quantifying plaque burden is needed. MR visualization of β-amyloid plaques has been accomplished in human *ex vivo* hippocampal samples using a T_2^*-weighted pulse sequence and

7.1 T scanner (Benveniste *et al.*, 1999). Jack *et al.* (2004) used a 9.4-T scanner and customized radiofrequency coil specific for imaging murine brain. The ability to directly visualize β-amyloid plaques using MRI is thought to be due to time-related iron accumulation (Jack *et al.*, 2004; Wadghiri *et al.*, 2004; Vanhoutte *et al.*, 2005). MRI is sensitive to these iron accumulations due to T_2 and T_2^* susceptibility effects that they cause, effectively spoiling the MR signal normally attained from the brain parenchyma. Hence, with sufficiently sensitive detection methodology, iron-loaded β-amyloid plaques can appear as signal voids in MR images. This typically is achieved by collecting high-resolution, high-SNR images using high field-strength scanners and customized radiofrequency hardware, and proper choice of pulse sequence and acquisition timing parameters (T_2- and T_2^*-weighting), giving high sensitivity to the iron susceptibility effects. Our detection scheme is unique in that it uses a combination of a clinical field-strength (3 T) scanner, customized gradient and radiofrequency coils for generating high-resolution, high-SNR images and a pulse sequence (3DFIESTA) with high SNR efficiency and excellent sensitivity to susceptibility contrast created by iron deposits. These technologies were previously optimized for imaging of single cells loaded with iron oxide nanoparticles for such applications as tracking metastatic cancer cells (Heyn *et al.*, 2006a, b). However, as shown here, this technology is also well

suited for detection of endogenous accumulation of iron deposits within diseases such as Alzheimer's disease and should allow tracking of β-amyloid plaque burden in individual animals over time.

One interesting MRI finding is that signal voids were detected in white matter with a similar frequency as in grey matter (Fig. 5C; not significantly different). We believe that the majority of these voids are iron-loaded plaques as revealed by histology and identifies a difference of our model compared with Alzheimer's disease in humans where plaques are more frequently found in grey matter. However, some voids may indicate an additional, as yet unidentified, pathological consequence of cholesterol feeding in our rabbits, or β-amyloid plaques in white matter regions of our rabbit brains may be more enriched with iron than those found in grey matter, thus being more easily detected with our iron-sensitive MR technique. At present, it is too early to interpret this finding with certainty.

The gradient coil supported use of a clinical field-strength scanner also opens the possibility of MRI's potential for detection of β-amyloid plaques in humans, as previously reported (Jack *et al.*, 2004). While significant technical challenges would have to be overcome, several areas of research hint that this might not be impossible. The availability of whole-body 7 T clinical scanners has led to significant SNR gains, and customized head/neck gradient coils are capable of generating high-resolution images (Chronik *et al.*, 2000). High-field head radiofrequency coils with high SNR efficiency are being developed (Avdievich and Hetherington, 2008), and parallel imaging techniques should lead to significant reductions in scan times (Weiger *et al.*, 2002). By minimizing field inhomogeneities, SNR-efficient, iron-sensitive pulse sequences such as 3DFIESTA may be implemented on these higher field-strength scanners. Successful imaging of β-amyloid plaques in humans, combined with structural neuroimaging measures of atrophy and neurofibrillary tangle burden could provide a comprehensive evaluation of Alzheimer's disease pathogenesis using one imaging modality.

In conclusion, we present a new survivable cholesterol-fed rabbit model of Alzheimer's disease based on titration of ingested cholesterol over long-time periods combined with a unique clinical field-strength MR technique for direct detection of the brain β-amyloid plaques. Future study of this model should provide invaluable information about the relationship between plasma cholesterol metabolism and Alzheimer's disease initiation and progression. Technical development of rabbit-specific MR technology should allow these effects to be non-invasively and longitudinally tracked in individual animals. This would significantly advance our ability to study the efficacy of interventions aimed at decreasing β-amyloid plaque burden in this animal model and the effects of cholesterol-lowering interventions on Alzheimer's disease development; ultimately with translation of these effects to Alzheimer's disease patients.

Supplementary material

Supplementary material is available at *Brain* online.

References

Avdievich NI, Hetherington HP. High-field head radiofrequency volume coils using transverse electromagnetic (TEM) and phased array technologies. NMR Biomed 2008 [Epub ahead of print].

Benveniste H, Einstein G, Kim KR, Hulette C, Johnson GA. Detection of neuritic plaques in Alzheimer's disease by magnetic resonance microscopy. Proc Natl Acad Sci USA 1999; 96: 14079–84.

Braakman N, Matysik J, van Duinen SG, Verbeek F, Schliebs R, de Groot HJ, et al. Longitudinal assessment of Alzheimer's beta-amyloid plaque development in transgenic mice monitored by in vivo magnetic resonance microimaging. J Magn Reson Imaging 2006; 24: 530–6.

Canevari L, Clark JB. Alzheimer's disease and cholesterol: the fat connection. Neurochem Res 2007; 32: 739–50.

Carr DB, Goate A, Phil D, Morris JC. Current concepts in the pathogenesis of Alzheimer's disease. Am J Med 1997; 103: 3S–10S.

Chronik BA, Alejski A, Rutt BK. Design and fabrication of a three-axis edge ROU head and neck gradient coil. Magn Reson Med 2000; 44: 955–63.

Corder EH, Saunders AM, Strittmatter WJ, Schmechel DE, Gaskell PC, Small GW, et al. Gene dose of apolipoprotein E type 4 allele and the risk of Alzheimer's disease in late onset families. Science 1993; 261: 921–3.

Curtain CC, Ali FE, Smith DG, Bush AI, Masters CL, Barnham KJ. Metal ions, pH, and cholesterol regulate the interactions of Alzheimer's disease amyloid-beta peptide with membrane lipid. J Biol Chem 2003; 278: 2977–82.

Daley SJ, Herderick EE, Cornhill JF, Rogers KA. Cholesterol-fed and casein-fed rabbit models of atherosclerosis. Part 1: differing lesion area and volume despite equal plasma cholesterol levels. Arterioscler Thromb 1994a; 14: 95–104.

Daley SJ, Klemp KF, Guyton JR, Rogers KA. Cholesterol-fed and casein-fed rabbit models of atherosclerosis. Part 2: differing morphological severity of atherogenesis despite matched plasma cholesterol levels. Arterioscler Thromb 1994b; 14: 105–41.

Ehehalt R, Keller P, Haass C, Thiele C, Simons K. Amyloidogenic processing of the Alzheimer beta-amyloid precursor protein depends on lipid rafts. J Cell Biol 2003; 160: 113–23.

Foster-Gareau P, Heyn C, Alejski A, Rutt BK. Imaging single mammalian cells with a 1.5 T clinical MRI scanner. Magn Reson Med 2003; 49: 968–71.

Gosche KM, Mortimer JA, Smith CD, Markesbery WR, Snowdon DA. Hippocampal volume as an index of Alzheimer neuropathology: findings from the Nun Study. Neurology 2002; 58: 1476–82.

Heyn C, Bowen CV, Rutt BK, Foster PJ. Detection threshold of single SPIO-labeled cells with FIESTA. Magn Reson Med 2005; 53: 312–20.

Heyn C, Ronald JA, Mackenzie LT, MacDonald IC, Chambers AF, Rutt BK, et al. In vivo magnetic resonance imaging of single cells in mouse brain with optical validation. Magn Reson Med 2006a; 55: 23–9.

Heyn C, Ronald JA, Ramadan SS, Snir JA, Barry AM, MacKenzie LT, et al. In vivo MRI of cancer cell fate at the single-cell level in a mouse model of breast cancer metastasis to the brain. Magn Reson Med 2006b; 56: 1001–10.

Hofman A, Ott A, Breteler MM, Bots ML, Slooter AJ, van Harskamp F, et al. Atherosclerosis, apolipoprotein E, and prevalence of dementia and Alzheimer's disease in the Rotterdam Study. Lancet 1997; 349: 151–4.

Hulette CM, Welsh-Bohmer KA, Murray MG, Saunders AM, Mash DC, McIntyre LM. Neuropathological and neuropsychological changes in ''normal'' aging: evidence for preclinical Alzheimer disease in cognitively normal individuals. J Neuropathol Exp Neurol 1998; 57: 1168–74.

Jack CR Jr, Dickson DW, Parisi JE, Xu YC, Cha RH, O'Brien PC, et al. Antemortem MRI findings correlate with hippocampal neuropathology in typical aging and dementia. Neurology 2002; 58: 750–7.

Jack CR Jr, Garwood M, Wengenack TM, Borowski B, Curran GL, Lin J, et al. In vivo visualization of Alzheimer's amyloid plaques by magnetic resonance imaging in transgenic mice without a contrast agent. Magn Reson Med 2004; 52: 1263–71.

Jack CR Jr, Petersen RC, O'Brien PC, Tangalos EG. MR-based hippocampal volumetry in the diagnosis of Alzheimer's disease. Neurology 1992; 42: 183–8.

Jack CR Jr, Wengenack TM, Reyes DA, Garwood M, Curran GL, Borowski BJ, et al. In vivo magnetic resonance microimaging of individual amyloid plaques in Alzheimer's transgenic mice. J Neurosci 2005; 25: 10041–8.

Jicha GA, Parisi JE, Dickson DW, Johnson K, Cha R, Ivnik RJ, et al. Neuropathologic outcome of mild cognitive impairment following progression to clinical dementia. Arch Neurol 2006; 63: 674–81.

Josephs KA, Whitwell JL, Ahmed Z, Shiung MM, Weigand SD, Knopman DS, et al. Beta-amyloid burden is not associated with rates of brain atrophy. Ann Neurol 2008; 63: 204–12.

Khachaturian ZS. Diagnosis of Alzheimer's disease. Arch Neurol 1985; 42: 1097–105.

Kivipelto M, Helkala EL, Hanninen T, Laakso MP, Hallikainen M, Alhainen K, et al. Midlife vascular risk factors and late-life mild cognitive impairment: a population-based study. Neurology 2001a; 56: 1683–9.

Kivipelto M, Helkala EL, Laakso MP, Hanninen T, Hallikainen M, Alhainen K, et al. Midlife vascular risk factors and Alzheimer's disease in later life: longitudinal, population based study. Br Med J 2001b; 322: 1447–51.

Knopman DS, Parisi JE, Salviati A, Floriach-Robert M, Boeve BF, Ivnik RJ, et al. Neuropathology of cognitively normal elderly. J Neuropathol Exp Neurol 2003; 62: 1087–95.

Li G, Larson EB, Sonnen JA, Shofer JB, Petrie EC, Schantz A, et al. Statin therapy is associated with reduced neuropathologic changes of Alzheimer disease. Neurology 2007; 69: 878–85.

Morris JC, Price AL. Pathologic correlates of nondemented aging, mild cognitive impairment, and early-stage Alzheimer's disease. J Mol Neurosci 2001; 17: 101–18.

Pappolla MA, Bryant-Thomas TK, Herbert D, Pacheco J, Fabra Garcia M, Manjon M, et al. Mild hypercholesterolemia is an early risk factor for the development of Alzheimer amyloid pathology. Neurology 2003; 61: 199–205.

Petrella JR, Coleman RE, Doraiswamy PM. Neuroimaging and early diagnosis of Alzheimer disease: a look to the future. Radiology 2003; 226: 315–36.

Ronald JA, Walcarius R, Robinson JF, Hegele RA, Rutt BK, Rogers KA. MRI of early- and late-stage arterial remodeling in a low-level cholesterol-fed rabbit model of atherosclerosis. J Magn Reson Imaging 2007; 26: 1010–9.

Schott JM, Price SL, Frost C, Whitwell JL, Rossor MN, Fox NC. Measuring atrophy in Alzheimer disease: a serial MRI study over 6 and 12 months. Neurology 2005; 65: 119–24.

Simons M, Keller P, De Strooper B, Beyreuther K, Dotti CG, Simons K. Cholesterol depletion inhibits the generation of beta-amyloid in hippocampal neurons. Proc Natl Acad Sci USA 1998; 95: 6460–4.

Sparks DL, Hunsaker JC 3rd, Scheff SW, Kryscio RJ, Henson JL, Markesbery WR. Cortical senile plaques in coronary artery disease, aging and Alzheimer's disease. Neurobiol Aging 1990; 11: 601–7.

Sparks DL, Sabbagh MN, Connor DJ, Lopez J, Launer LJ, Browne P, et al. Atorvastatin for the treatment of mild to moderate Alzheimer disease: preliminary results. Arch Neurol 2005; 62: 753–7.

Sparks DL, Scheff SW, Hunsaker JC 3rd, Liu H, Landers T, Gross DR. Induction of Alzheimer-like beta-amyloid immunoreactivity in the brains of rabbits with dietary cholesterol. Exp Neurol 1994; 126: 88–94.

Sparks DL, Schreurs BG. Trace amounts of copper in water induce beta-amyloid plaques and learning deficits in a rabbit model of Alzheimer's disease. Proc Natl Acad Sci USA 2003; 100: 11065–9.

Streit WJ, Sparks DL. Activation of microglia in the brains of humans with heart disease and hypercholesterolemic rabbits. J Mol Med 1997; 75: 130–8.

Vanhoutte G, Dewachter I, Borghgraef P, Van Leuven F, Van der Linden A. Noninvasive in vivo MRI detection of neuritic plaques associated with iron in APP[V717I] transgenic mice, a model for Alzheimer's disease. Magn Reson Med 2005; 53: 607–13.

Vemuri P, Whitwell JL, Kantarci K, Josephs KA, Parisi JE, Shiung MS, et al. Antemortem MRI based STructural Abnormality iNDex (STAND)-scores correlate with postmortem Braak neurofibrillary tangle stage. Neuroimage 2008; 42: 559–67.

Villemagne VL, Rowe CC, Macfarlane S, Novakovic KE, Masters CL. Imaginem oblivionis: the prospects of neuroimaging for early detection of Alzheimer's disease. J Clin Neurosci 2005; 12: 221–30.

Wadghiri YZ, Blind JA, Duan X, Moreno C, Yu X, Joyner AL, et al. Manganese-enhanced magnetic resonance imaging (MEMRI) of mouse brain development. NMR Biomed 2004; 17: 613–9.

Weiger M, Pruessmann KP, Boesiger P. 2D SENSE for faster 3D MRI. Magma 2002; 14: 10–9.

Whitmer RA, Sidney S, Selby J, Johnston SC, Yaffe K. Midlife cardiovascular risk factors and risk of dementia in late life. Neurology 2005; 64: 277–81.

Wolozin B, Kellman W, Ruosseau P, Celesia GG, Siegel G. Decreased prevalence of Alzheimer disease associated with 3-hydroxy-3-methylglutaryl coenzyme A reductase inhibitors. Arch Neurol 2000; 57: 1439–43.

Yip CM, Elton EA, Darabie AA, Morrison MR, McLaurin J. Cholesterol, a modulator of membrane-associated Abeta-fibrillogenesis and neurotoxicity. J Mol Biol 2001; 311: 723–34.